Aerospace Science and Technology 55 (2016) 1–9

Contents lists available at ScienceDirect

Aerospace Science and Technology

www.elsevier.com/locate/aescte

Direct image-based visual servoing of free-floating space manipulators

Javier Pérez Alepuz [a], M. Reza Emami [b,c,*], Jorge Pomares [a]

[a] University of Alicante, POBox 99, 03080, Alicante, Spain
[b] Division of Space Technology, Luleå University of Technology, Rymdcampus, E10, Kiruna 98128, Sweden
[c] University of Toronto Institute for Aerospace Studies, 4925 Dufferin Street, Toronto, Ontario M3H 5T6, Canada

ARTICLE INFO

Article history:
Received 20 January 2016
Received in revised form 13 April 2016
Accepted 11 May 2016
Available online 16 May 2016

Keywords:
Visual servoing
Free-floating manipulator
Space manipulator
Model-based control

ABSTRACT

This paper presents an image-based controller to perform the guidance of a free-floating robot manipulator. The manipulator has an eye-in-hand camera system, and is attached to a base satellite. The base is completely free and floating in space with no attitude control, and thus, freely reacting to the movements of the robot manipulator attached to it. The proposed image-based approach uses the system's kinematics and dynamics model, not only to achieve a desired location with respect to an observed object in space, but also to follow a desired trajectory with respect to the object. To do this, the paper presents an optimal control approach to guiding the free-floating satellite-mounted robot, using visual information and considering the optimization of the motor commands with respect to a specified metric along with chaos compensation. The proposed controller is applied to the visual control of a four-degree-of-freedom robot manipulator in different scenarios.

1. Introduction

The research and development of robot manipulators on satellites for space operations has had a remarkable growth within the past few years. These manipulators are especially suited for precise, complex, or even dangerous tasks for astronauts. Currently, the utilization of the robot manipulators mounted on satellites can be summarized into six categories [1]: i) assembly, maintenance and repair; ii) spacecraft deployment, release and retrieve; iii) extravehicular activity support; iv) inspection; v) refueling; and vi) multi-arm cooperation. Regarding the base spacecraft, two types of operations are considered and studied [2]: free-floating case, where the base is completely free and floating in space with no attitude control; and thus, freely reacting to the movements of the manipulator attached to it; and free-flying case, where the base is actively controlled, and thus, the system's attitude and position can be controlled. In this paper, the free-floating case is considered, where the robot manipulator must be positioned with respect to a tumbling object from which a set of visual features can be extracted by the eye-in-hand camera system. The classical approach to dealing with this kind of situations is divided into four phases [1]: i) observing and planning; ii) final approaching; iii) impact and capture; and iv) post-capturing stabilization; usually knowing all the parameters of the target object, but there are also some works that deal with the capturing and stabilization of objects with unknown dynamics [3]. The control strategy discussed in this paper will focus on observing and approaching the tumbling object. This paper presents a new image-based visual servoing approach, using the kinematics and dynamics model of this kind of robots, not only to achieve a desired location with respect to the observed object in the space, but also to follow a desired trajectory with respect to the tumbling object.

Classical visual servoing systems allow for carrying out point-to-point motion of a robot using visual information. A well-known classification of this kind of control systems divides them into position-based and image-based visual servoing [4]. In the first category, image features are extracted from the captured image and a model of the scene, and the target is used to determine its pose with respect to the frame attached to the camera. However, in the second category, pose estimation is omitted, and the control law is directly expressed in the image space. In this paper, visual information is used to perform the guidance of a free-floating satellite-mounted robot (FFSMR). In this case, an image-based approach allows for defining the control law directly in the image space, and does not need precise calibration and modeling (only a set of visual features must be extracted from the observed object as described through the paper). This approach is proposed in order to perform the guidance of the FFSMR with respect to space objects, such as orbital debris, small asteroids, or defunct spacecraft. Classical image-based visual servoing assumes that the

* Corresponding author at: Division of Space Technology, Luleå University of Technology, Rymdcampus, E10, Kiruna 98128, Sweden.
E-mail addresses: jpalepuz@ua.es (J.P. Alepuz), reza.emami@ltu.se (M.R. Emami), jpomares@ua.es (J. Pomares).

http://dx.doi.org/10.1016/j.ast.2016.05.012
1270-9638/

robot is a perfect positioning device. This type of control does not take into account the system dynamics, which is not suitable when the robot executes fast and/or accurate movements. Few proposed image-based controllers take into account the non-linear dynamics model of robotic arms, usually referred to as direct visual servoing. By means of direct visual servoing, the internal control loop of servomotors is removed, so the visual servo control law directly provides the torque to be applied to the robot joints. Additionally, integrating the FFSMR dynamics in the visual controller allows for obtaining a relation between joint speeds and end-effector motion of the robot manipulator taking into account the base attitude disturbance during the tracking. As shown in the results section, the use of this approach during the tracking allows for increasing the tracking performance with respect to classical image-based visual servoing systems.

A great number of visual servoing approaches, proposed up to now to perform the guidance of in-orbit robot manipulators, use a position-based approach. In [5], a 3D model-based tracking is used for a space rendezvous mission. In this case, a vision-based navigation is proposed using a 21/2 D visual servoing approach [6], without considering the system dynamics. In [7], the same researchers present a generic tracking and pose estimation method suited for complex, textured or untextured objects in deep space environments, for space rendezvous and space debris removal purposes. Within this last topic we should mention the work presented in [8], where an estimation method of relative pose based on stereo vision is presented for the final phase of the rendezvous and docking of non-cooperative satellites. In [9], relative navigation method for rendezvous and docking of an unknown tumbling object using a monocular camera is presented. Two extended Kalman filters with different models are used for relative orbit estimation in far range and relative position and attitude estimation in close range. Within this topic, it is worth mentioning the works of Aghili (see e.g. [3,10]), which describe a combined prediction and motion planning approach for robotic arms during the phase of pre- and post-grasping of tumbling objects with unknown dynamics. A Kalman filter is employed to estimate the object dynamics used for the robot path planning. A position-based approach is used utilizing the system dynamics. In order to perform the in-orbit robot guidance without estimating the relative pose between the robot and the observed object, several researchers have proposed the use of image-based approaches. In [11], a classical image-based visual servoing applied to the Japanese Engineering Test Satellite VII (ETSVII) is proposed. As it is described in [12], multiple tasks can be controlled in a hierarchical manner. The last work presents a priority-based redundancy resolution at the velocity level. This method chooses one task as primary, and projects the other tasks (secondary, tertiary, etc.) into the null space of the primary task derivative. In [13], a classical image-based visual servoing approach is employed for the guidance of a mounted dual-arm space robot. The work is designed to complete the task of servoing the robot's end-effectors to the desired pose, while regulating the orientation of the base-satellite. The visual task is defined as a primary task, while regulating the attitude of the base satellite to zero is defined as a secondary task without considering the system dynamics. Image-based control is also used in the experimental test-bed proposed in [14]. The paper shows that it is possible to evaluate the elastic properties of a multibody manipulator, thanks to the analysis of the acquired images. In [15], a classical image-based, a position-based, and a switching approach are presented for autonomous satellite capture using an on-board manipulator with binocular hand-eye cameras without considering the system dynamics. In [16], the previous approach is simulated taking into account the system dynamics; however, a classical indirect implementation is considered. None of the previous implementations of image-based visual servoing systems for FFSMR considers a direct visual control approach. The need for integrating the system dynamics in the guidance of FFSMR using image information is discussed in works such as [15] and [17]. These works describe a set of ground verification systems, which can experimentally verify and test the reliability of visual servoing control systems and path planning of space robots. In [18], a direct image-based visual servoing approach for guiding a FFSMR using an eye-in-hand camera system is proposed. In this case, an inverse dynamics controller is developed to lock the projection of a feature point at a desired constant position on the image plane from an initial one. Contrary to previous papers, using the direct visual servoing approach proposed in this paper, the FFSMR is able to track a desired image trajectory with respect to an observed object (not only a positioning task). Additionally, this paper proposes an optimal control approach to guide the FFSMR using visual information. This approach allows for tracking trajectories considering the optimization of the motor commands with respect to a specified metric. As shown in the experimental results, the use of this controller, jointly with the integration of a chaos compensation technique, allows to increase the tracking precision and to reduce the base attitude disturbance during the tracking. The proposed controller is applied to the direct visual control of a FFSMR during the tracking of image trajectories.

The paper is divided into the following sections. First, the kinematics and dynamics of the FFSMR is defined. Next, the proposed optimal visual system is explained in Section 3. Section 4 discusses the simulation results, and Section 5 makes few concluding remarks.

2. Kinematics and dynamics of the FFSMR

2.1. System architecture and assumptions

Fig. 1 represents the main components of the FFSMR. With $q \in \Re^n$ are represented the generalized joint coordinates of the robot manipulator (in our case, $n = 4$). Frame $\{B\}$ is attached to the base satellite. The inertial coordinate frame is called $\{I\}$. The end-effector frame, $\{E\}$, is attached to the manipulator end-effector, and frame $\{C\}$ is the camera frame (attached to the camera). The camera extracts k visual feature points from the observed object $s = [\mathfrak{f}_{1x}, \mathfrak{f}_{1y}, \mathfrak{f}_{2x}, \mathfrak{f}_{2y}, \ldots, \mathfrak{f}_{kx}, \mathfrak{f}_{ky}]^{\mathrm{T}} \in \Re^{2k}$. Therefore, the image-based direct visual controller must perform the FFSMR guidance to track the desired trajectory in the image space, $s_d(t)$.

As previously indicated, this paper defines a direct visual servoing system applied to a FFSMR for the tracking of image trajectories. Additionally, in this paper, we assume that:

a) The FFSMR will track an image trajectory defined with respect to a target object from which four visual features points can be extracted, i.e., $k = 4$. The presented controller can be easily extended to employ other kinds of visual primitive to perform the guidance (only the interaction matrix employed throughout the paper depends on the considered primitive [4]).
b) An eye-in-hand camera system is employed; therefore, a constant relation between the camera coordinate frame and the robot end-effector frame is considered.
c) The target undergoes constant linear and angular motion and its angular momentum is known in advance. An estimation can be obtained using previous works such as [19,20].
d) There are no external forces acting on the entire system. No gas-jet thrusters are used on the base satellite.
e) The capturing phase is not considered in this paper, therefore, there are no interaction forces between the FFSMR and the observed object.

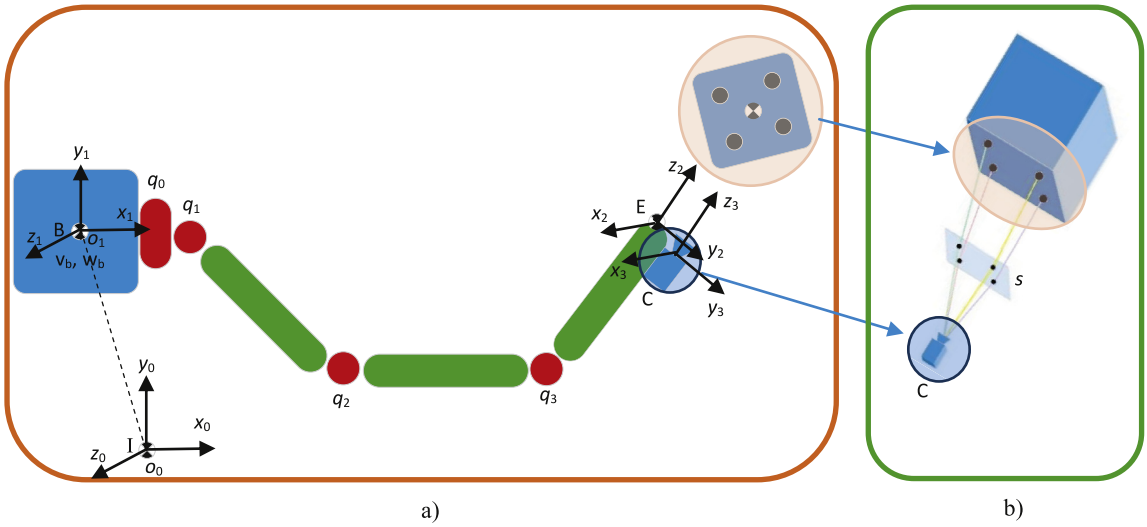

Fig. 1. Schematic representation of a) the FFSMR, b) the vision system.

2.2. FFSMR dynamics

The equations of motion of an n-degree-of-freedom (n-dof) FFSMR can be written as [21]:

$$\begin{bmatrix} F_b \\ \tau \end{bmatrix} = \begin{bmatrix} M_{bb} & M_{bm} \\ M_{bm}^{\mathrm{T}} & M_{mm} \end{bmatrix} \begin{bmatrix} \ddot{x}_b \\ \ddot{q} \end{bmatrix} + \begin{bmatrix} c_b \\ c_m \end{bmatrix} \tag{1}$$

where $\ddot{q} \in \Re^n$ is the set of joint accelerations, $\ddot{x}_b = [\dot{v}_b^{\mathrm{T}} \ \dot{\omega}_b^{\mathrm{T}}]^{\mathrm{T}} \in \Re^6$ denotes the absolute linear and angular accelerations of the base satellite expressed in the inertial coordinate frame, $M_{bb} \in \Re^{6\times 6}$ is the inertia matrix of the satellite, $M_{bm} \in \Re^{6\times n}$ is the coupled inertia matrix of the satellite and the manipulator, $M_{mm} \in \Re^{n\times n}$ is the inertia matrix of the manipulator; c_b and $c_m \in \Re^6$ are velocity/displacement-dependent, non-linear terms for the base and manipulator, respectively, $F_b \in \Re^6$ is the force and moment exerted on the base satellite, and $\tau \in \Re^n$ is the applied joint torque on the robot manipulator. The FFSMR is freely floating in space; therefore, the external wrench on the satellite and the manipulator end-effector is assumed to be zero. The motion of the FFSMR is governed only by the applied torque on the manipulator joints, $F_b = 0$. Hence, equation (1) can be written in the following compact form:

$$M_{mm}^* \ddot{q} + H^* = \tau \tag{2}$$

where $M_{mm}^* \in \Re^{n\times n}$ is the generalized inertia matrix and $H^* \in \Re^n$ is the generalized Coriolis and centrifugal matrix, defined explicitly as:

$$M_{mm}^* = M_{mm} - M_{bm}^{\mathrm{T}} M_{bb}^{-1} M_{bm} \tag{3}$$

$$H^* = c_m - M_{bm}^{\mathrm{T}} M_{bb}^{-1} c_b \tag{4}$$

The linear and angular momenta of the system $(\ell^{\mathrm{T}}, \Psi^{\mathrm{T}})^{\mathrm{T}} \in \Re^6$ are equal to:

$$\begin{bmatrix} \ell \\ \Psi \end{bmatrix} = M_{bb}\dot{x}_b + M_{bm}\dot{q} \tag{5}$$

where $\dot{q} \in \Re^n$ represents the robot manipulator joint speeds, and $\dot{x}_b = [v_b^{\mathrm{T}} \ \omega_b^{\mathrm{T}}]^{\mathrm{T}} \in \Re^6$ denotes the absolute linear and angular velocities of the base satellite expressed in the inertial coordinate frame. The relationship between the joint speeds and the corresponding end-effector's absolute linear and angular velocities can be expressed through differential kinematics. For the FFSMR,

$$\dot{x}_e = J_m\dot{q} + J_b\dot{x}_b \tag{6}$$

where $\dot{x}_e \in \Re^6$ is the linear and angular velocity of the manipulator end-effector in the inertial frame, $J_m \in \Re^{6\times n}$ is the manipulator Jacobian matrix, and $J_b \in \Re^{6\times 6}$ is the Jacobian matrix for the base satellite. Combining (6) and (5) yields an equation directly relating the joint speeds and end-effector motion of the robot manipulator [21]:

$$\dot{x}_e = J_g\dot{q} + \dot{x}_{ge} \tag{7}$$

$$J_g = J_m - J_b M_{bb}^{-1} M_{bm} \tag{8}$$

$$\dot{x}_{ge} = J_b M_{bb}^{-1} \begin{bmatrix} \ell \\ \Psi \end{bmatrix} \tag{9}$$

where J_g is the Generalized Jacobian Matrix, and $\dot{x}_{ge}$, is an offset velocity due to the non-zero momentum. The visual servoing control techniques allow for the control of manipulator joints using k visual features, typically using an eye-in-hand configuration, where a camera is held by the end-effector. The relationship between velocities in the camera image space, $\dot{s}_r$, and end-effector motion, $\dot{x}_e$, is expressed by:

$$\dot{s}_r = L_s\dot{x}_e \tag{10}$$

where $L_s \in \Re^{2k\times 6}$ is the interaction matrix [1], and $s_r = [f_{1x}, f_{1y}, f_{2x}, f_{2y}, \ldots, f_{kx}, f_{ky}]^{\mathrm{T}} \in \Re^{2k}$ is a vector of the k extracted image feature points. From (10) and (7), the image space velocity $\dot{s}_r$ can be related to joint speeds $\dot{q}$ by means of the following relationship:

$$\dot{s}_r = L_s J_g\dot{q} + L_s\dot{x}_{ge} = L_J\dot{q} + \dot{s}_{ge} \tag{11}$$

where L_J is the Jacobian matrix mapping from joint space to image space. This matrix relates differential changes in joint configuration of the robot to differential changes in the observed image feature parameters. Additionally, $\dot{s}_{ge}$ is considered as the projection in the image space of the velocity $\dot{x}_{ge}$. The image acceleration or second derivative of s_r is obtained by differentiating Equation (11) with respect to time:

$$\ddot{s}_r = L_J\ddot{q} + \dot{L}_J\dot{q} + \ddot{s}_{ge} \tag{12}$$

The variable $\ddot{s}_r$ denotes the reference image accelerations that will be employed by the optimal controller proposed in Section 3.

3. Optimal control approach

3.1. Direct control of the FFSMR

This paper considers a system with m constrains that represent the task for the FFSMR to be executed. The time derivate of these constraints is represented by the following equation:

$$A(q,\dot{q},t)\ddot{q} = b(q,\dot{q},t) \tag{13}$$

where $A(q,\dot{q},t) \in \Re^{m\times n}$ and $b(q,\dot{q},t) \in \Re^{m\times 1}$. In order to reduce the energy and fuel required for performing the visual servoing task, the proposed optimal controller is designed to minimize the control torque for the FFSMR, taking into account the following function cost:

$$\Omega(t) = \tau^{\mathrm{T}} W(t)\tau \tag{14}$$

where $W(t)$ is a time-dependent weight matrix. By defining $z = W^{1/2}\tau = W^{1/2}(M^*_{mm}\ddot{q} + H^*)$, it is possible to derive the joint accelerations $\ddot{q} = (M^*_{mm})^{-1}(W^{-1/2}z - H^*)$. Taking into account the constraints defined in Equation (13):

$$A\left(M^*_{mm}\right)^{-1} W^{-1/2} z = b + A\left(M^*_{mm}\right)^{-1} H^* \tag{15}$$

The vector z which minimizes $\Omega(t) = z^{\mathrm{T}}z$ while fulfilling Equation (15) is given by $z = (A(M^*_{mm})^{-1}W^{-1/2})^{+}(b + A(M^*_{mm})^{-1}H^*)$, and as the joint torque is given by $\tau = W^{-1/2}z$. To conclude, the control law that minimizes $\Omega(t)$ of the FFSMR based on the dynamics model expressed in Equation (2), while performing the task described in Equation (13), is given by:

$$\tau = W^{-1/2}\left(A\left(M^*_{mm}\right)^{-1} W^{-1/2}\right)^{+} \cdot \left(b + A\left(M^*_{mm}\right)^{-1} H^*\right) \tag{16}$$

where the symbol $+$ denotes the pseudo-inverse of a general matrix. As it can be seen in Equation (16), the matrix W is an important factor in the control law determining how the control efforts are distributed over the joints.

Equation (12), which relates the visual servoing task with the joint space, can be expressed into the form of Equation (13) as:

$$L_J\ddot{q} = \ddot{s}_r - \dot{L}_J\dot{q} - \ddot{s}_{ge} \tag{17}$$

This way, the task constrains are defined by the following relationships:

$$\begin{aligned} A &= L_J \\ b &= \ddot{s}_r - \dot{L}_J\dot{q} - \ddot{s}_{ge} \end{aligned} \tag{18}$$

Therefore, with the given definition of A and b, the optimal control will minimize the control torque for the joints while performing a tracking in the image space. The final control law can be obtained replacing these variables into the function that minimizes the motor signals described by Equation (16):

$$\begin{aligned} \tau = W^{-1/2}&\left(L_J\left(M^*_{mm}\right)^{-1} W^{-1/2}\right)^{+} \cdot \left(\ddot{s}_r - \dot{L}_J\dot{q} - \ddot{s}_{ge}\right. \\ &\left. + L_J\left(M^*_{mm}\right)^{-1} H^*\right) \end{aligned} \tag{19}$$

As it can be seen, the visual controller represented by (19) implicitly depends on the weighting matrix W, and different values of this matrix can simplify the product $L_J(M^*_{mm})^{-1}W^{-1/2}$, and consequently the control law. A proper choice practically would be $W = (M^*_{mm})^{-1}$.

The optimal control approach described in this section will be employed to track an image trajectory, taking into account the FFSMR dynamics. As discussed, the tracked trajectory is defined and expressed as a set of constraints following Equation (13) (see Equation (18)). Now, the definition of the reference control, $\ddot{s}_r$, is described considering an eye-in-hand camera system which extracts a set of k image feature points. The task description as a constraint is given by the following equation in the image space:

$$(\ddot{s}_d - \ddot{s}) + K_D(\dot{s}_d - \dot{s}) + K_P(s_d - s) = 0 \tag{20}$$

where $\ddot{s}_d$, $\dot{s}_d$ and s_d are the desired image space accelerations, velocities and positions, respectively. K_P and K_D are proportional and derivative gain matrices, respectively. This equation can be expressed in regards to image error in the following way:

$$\ddot{s}_d + K_D\dot{e}_s + K_P e_s = \ddot{s}_r \tag{21}$$

where e_s and $\dot{e}_s$ are the image error and the time derivative of the image error, respectively. As stated, the variable $\ddot{s}_r$ denotes the reference image accelerations of the proposed image space based controller. Substituting this variable into the dynamic visual servo controller, Equation (19), the control law is set by the following relationship:

$$\begin{aligned} \tau = W^{-1/2}&\left(L_J\left(M^*_{mm}\right)^{-1} W^{-1/2}\right)^{+} \cdot \left(\ddot{s}_d + K_D\dot{e}_s + K_P e_s - \dot{L}_J\dot{q}\right. \\ &\left. - \ddot{s}_{ge} + L_J\left(M^*_{mm}\right)^{-1} H^*\right) \end{aligned} \tag{22}$$

In order to demonstrate the asymptotic tracking of the control law (22), some operations must be done. First, the closed-loop behavior is computed using Equation (2) as:

$$\begin{aligned} M^*_{mm}\ddot{q} + H^* = W^{-1/2}&\left(L_J\left(M^*_{mm}\right)^{-1} W^{-1/2}\right)^{+}\left(\ddot{s}_d + K_D\dot{e}_s\right. \\ &\left. + K_P e_s - \dot{L}_J\dot{q} - \ddot{s}_{ge} + L_J\left(M^*_{mm}\right)^{-1} H^*\right) \end{aligned} \tag{23}$$

Equation (23) can be simplified by pre-multiplying its left and right sides by $(L_J(M^*_{mm})^{-1}W^{-1/2})W^{1/2}$:

$$L_J\ddot{q} = \ddot{s}_d + K_D\dot{e}_s + K_P e_s - \dot{L}_J\dot{q} - \ddot{s}_{ge} \tag{24}$$

Using the relationship expressed in (17), it can be concluded that:

$$\ddot{e}_s = -K_D\dot{e}_s - K_P e_s \tag{25}$$

Therefore, when L_J is full-rank an asymptotic tracking is achieved by the visual servo controller expressed in Equation (19) for the tracking of an image trajectory.

3.2. Optimal control of the FFSMR with chaos compensation

Section 4 will evaluate the proposed controller during the tracking of repetitive and non-repetitive trajectories. When a visual servoing system is applied for the tracking of a repetitive image trajectory a chaotic joint behavior can be achieved. This behavior is obtained when the robot's end-effector tracks the image trajectory correctly, but an unpredictable and non-periodic motion is generated in the joint space. In general, when a chaotic behavior is obtained in the joint space, joint trajectories have a large number of unstable periodic orbits embedded. This non-repeatability in the joint space limits the practical applications of the visual controller. In the previous works [22], chaos compensation was integrated in classical direct visual controllers to obtain a periodic joint trajectory when the robot's end-effector also tracks a periodic image trajectory. This last aspect guarantees a smoother joint behavior, and increases the safety by obtaining predictable trajectories. In this paper, the chaos compensation is also integrated in the FFSMR controller in order to decrease the torque required to perform the guidance, consequently reducing the base attitude disturbance. To do this, a Delayed Feedback Control (DFC) method will be integrated in the controller. The DFC method generates a perturbation proportional to the difference between the current joint velocities and the joint velocities delayed by one period. The control action

Table 1
Dynamic parameters of the FFSMR.

Base	Mass (kg)	Side (m)	Inertia (kg m^2)		
			I_x	I_y	I_z
	60	0.3	22.5	22.5	22.5

Arm	Mass (kg)	Length (m)	Inertia (kg m^2)		
			I_x	I_y	I_z
Link 1	5	0.012	0.01	0.031	0.031
Link 2	1.75	0.124	0.002301	0.000981	0.002601
Link 3	0.8	0.152	0.001673	0.001656	0.001902
Link 4	0.5	0.099	0.0004802	0.0002	0.000546

or perturbation of the DFC controller vanishes when the stabilization of the target orbit is achieved. The resulting control law with chaos compensation is:

$$\tau = M^*_{mm}\lambda\big(q(t-\varepsilon)-q(t)\big) + W^{-1/2}\big(L_J\big(M^*_{mm}\big)^{-1}W^{-1/2}\big)^{+} \cdot \big(\ddot{s}_d + K_D\dot{e}_s + K_P e_s - \dot{L}_J\dot{q} - \ddot{s}_{ge} + L_J\big(M^*_{mm}\big)^{-1}H^*\big) \quad (26)$$

where λ is a constant gain to be determined, and ε is the feedback time-delay. The adjustment of the constants λ and ε is performed by using the algorithm described in [22]. By choosing an appropriate value of the control gain, λ, the target orbit can be stabilized. Using these values, the system under control automatically settles on the target periodic motion, and the stability of this motion is maintained with only small perturbations [23].

4. Simulations

This section describes simulations for the tracking of image trajectories considering the proposed direct visual servo controller. Table 1 lists the dynamic parameters employed in the simulation of the FFSMR. The robot manipulator's dynamic parameters are extracted from the 4-dof robot described in [24]. The robot is guided by an eye-in-hand camera system. The parameters of a Gigabit Ethernet TM6740GEV camera is considered, which acquires 200 images every second with a resolution of 1280×1024pixels. The eye-in-hand camera extracts four visual features from the workspace. These point features are obtained from the pattern represented in Fig. 1. The proportional and derivative matrices employed in the experiments are $K_P = diag(0.1)$ and $K_D = diag(0.5)$. Additionally, the weighting matrix is selected as $W = (M^*_{mm})^{-1}$. These values are considered in all the simulations presented in this section.

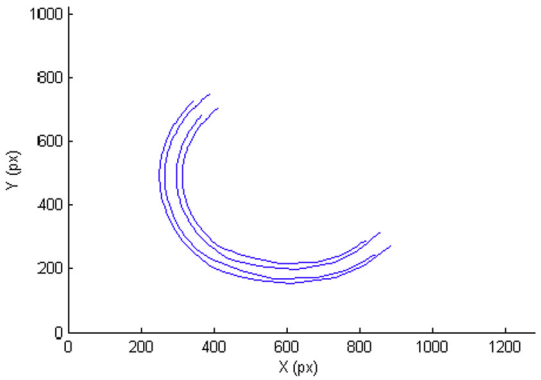

Fig. 2. Desired image trajectory. Experiment 1.

4.1. Tracking of an image trajectory

This experiment evaluates the tracking of the desired image trajectory indicated in Fig. 2. This figure represents the trajectory to be tracked for the four visual features extracted by the eye-in-hand camera system. Using the proposed controller, the end-effector trajectory in the 3D space represented in Fig. 3.a is obtained. In the beginning of the experiment, the robot's end-effector is not located at the desired trajectory. Therefore, the robot converges during the first iterations towards it (approaching phase) and continues the tracking of the desired trajectory. Fig. 3.b represents in blue the image error module during the experiment, $e = s - s_d$. From the Figure, the error remains low and decreases during the tracking. In order to highlight the necessity of integrating the system dynamics in the controller, a classical indirect visual servoing system [25] is also employed for the tracking of the trajectory presented in Fig. 2. Fig. 3.b represents, in red, the image error module obtained during the tracking by using the classical controller. As shown, the error is greater because the classical controller does not take into account the system dynamics and the base attitude disturbance during the tracking. The torque generated by the proposed direct controller during the tracking is shown in Fig. 4.a. Fig. 4.b represents the FFSMR during the tracking of the trajectory.

4.2. Tracking of a circular trajectory

This experiment evaluates the tracking of a planar and circular trajectory for the robot end-effector defined by the following equation:

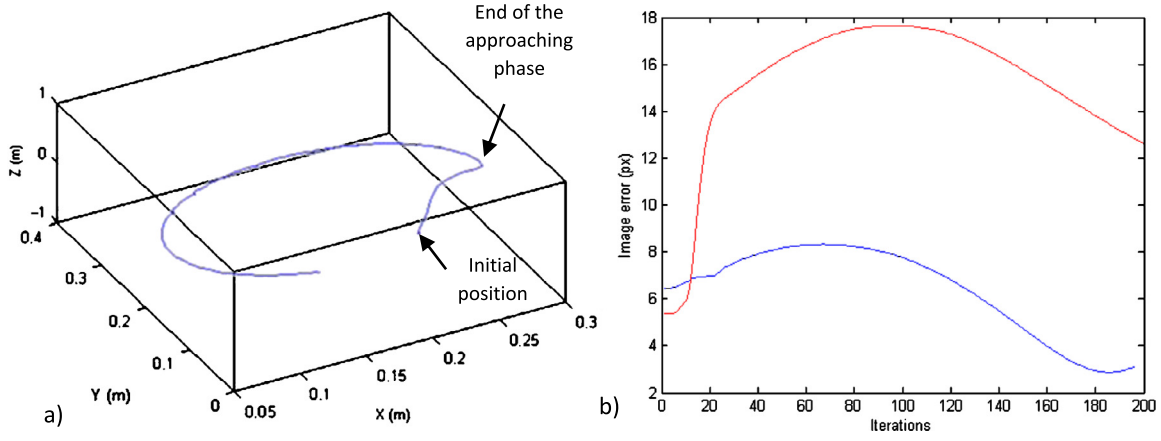

Fig. 3. a) 3D trajectory of the manipulator end-effector during the tracking. b) Image error using the proposed approach (bottom) and using classical image-based control (top). Experiment 1.

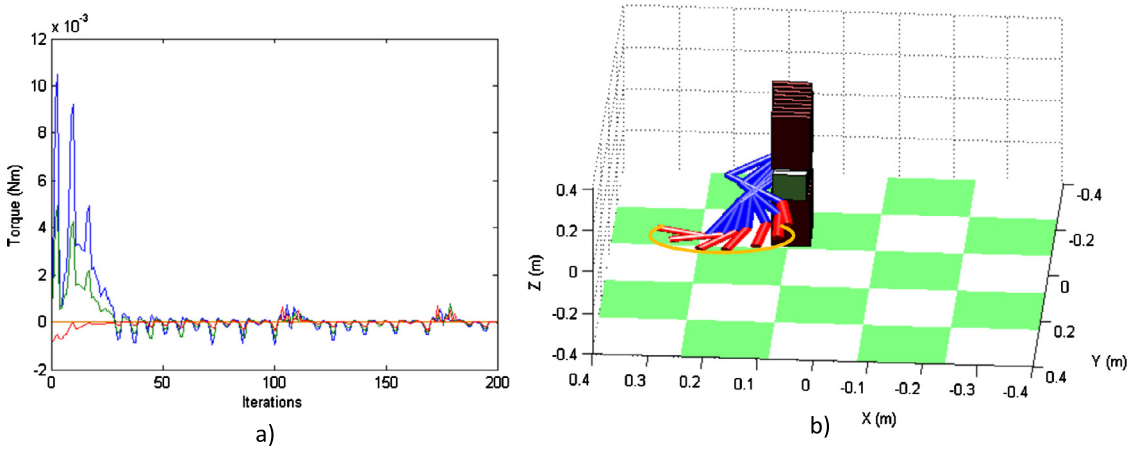

Fig. 4. a) Torque during the tracking. b) 3D trajectory of the FFSMR. Experiment 1.

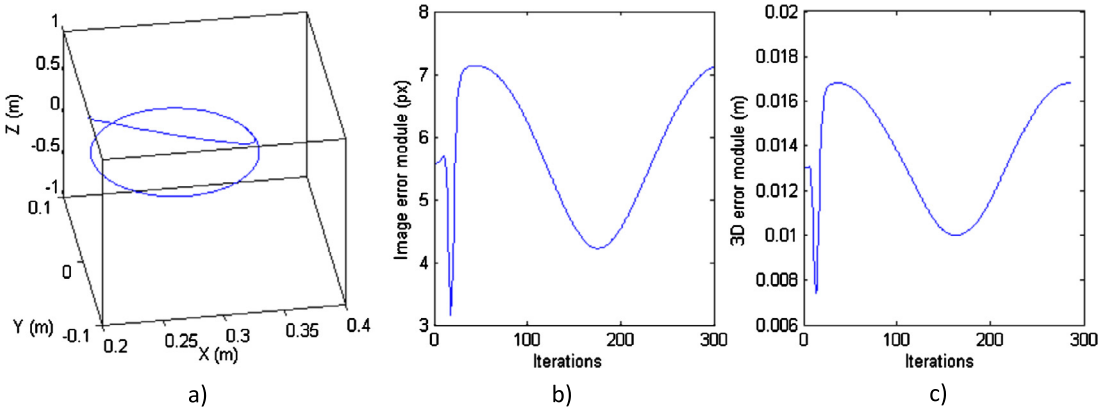

Fig. 5. a) 3D trajectory of the robot manipulator end-effector. b) Image error module. c) 3D error module. Experiment 2.

$$\begin{bmatrix} x_{xd} \\ y_{yd} \end{bmatrix} = \begin{bmatrix} 0.2 + 0.01\cos(0.02\pi t) \\ 0.02 + 0.01\sin(0.02\pi t) \end{bmatrix} \tag{27}$$

The tracking of this circular trajectory allows for evaluating the controller with and without the integration of the chaos controller mentioned in Section 3.2. Fig. 5.a represents the circular 3D trajectory described by the robot end-effector during the experiment. To observe the tracking precision more clearly, Fig. 5.b and Fig. 5.c show the image error module and the 3D Cartesian error module during the experiment, respectively. As it can be seen, these errors remain low during the experiment, and a correct tracking is carried out. These results are obtained by integrating the chaos controller. Similar results are obtained without the integration of the chaos controller. In order to observe the difference between these two strategies more clearly, the joint behavior is shown in Fig. 6 and Fig. 7. Fig. 6 represents the joint torque generated by the controller with and without chaos control. As it can be seen, lower torque values are obtained by integrating the chaos compensation in the controller. This effect can also be observed in the 3D trajectory described by the FFSMR during the tracking (Fig. 7). Fig. 7.a represents a sampling of the robot joint configurations employed during the tracking. As this figure shows, the joint configuration varies and a chaotic and unpredictable behavior is obtained in the joint space. A smoother and repetitive joint behavior is obtained in Fig. 7.b with the use of the chaos compensation.

4.3. Tracking of a repetitive and irregular trajectory

This experiment consists of the tracking of the repetitive and irregular trajectory in the image space that is shown in Fig. 8. From the control law stated in Equation (22), when $W = (M^*_{mm})^{-2}$, the following expression can be obtained for the controller, which represents a direct visual controller using inversion of the dynamic model:

$$\tau = M^*_{mm}(L_J)^+ \cdot \left(\ddot{s}_d + K_D\dot{e}_s + K_P e_s - \dot{L}_J\dot{q} - \ddot{s}_{ge} + L_J\left(M^*_{mm}\right)^{-1}H^*\right) \tag{28}$$

Fig. 9 evaluates the tracking of the desired image trajectory represented in Fig. 8 using both controllers, the one stated in Equation (28) and the one used in the previous experiments (Equation (22) and $W = (M^*_{mm})^{-1}$). In both cases, the chaos compensation method is integrated. As Fig. 9 shows, lower image and 3D errors are obtained using the proposed controller, $W = (M^*_{mm})^{-1}$, with respect to the one obtained when $W = (M^*_{mm})^{-2}$. Both controllers achieve the correct tracking, but a better image and 3D behavior is obtained with the proposed controller.

5. Conclusions

In contrast with the previous indirect image-based visual servoing approaches proposed up to now to perform the guidance of FFSMR, this paper presents a new direct image-based visual servoing system that takes into account the system kinematics and dynamics. The proposed controller allows the robot not only to achieve a given location from an initial one, but also to perform the tracking of a desired image trajectory. The proposed approach considers the optimization of the motor commands with respect to a specified metric defined by the user. Additionally, a chaos compensator is integrated in the proposed controller to improve the joint behavior during the tracking.

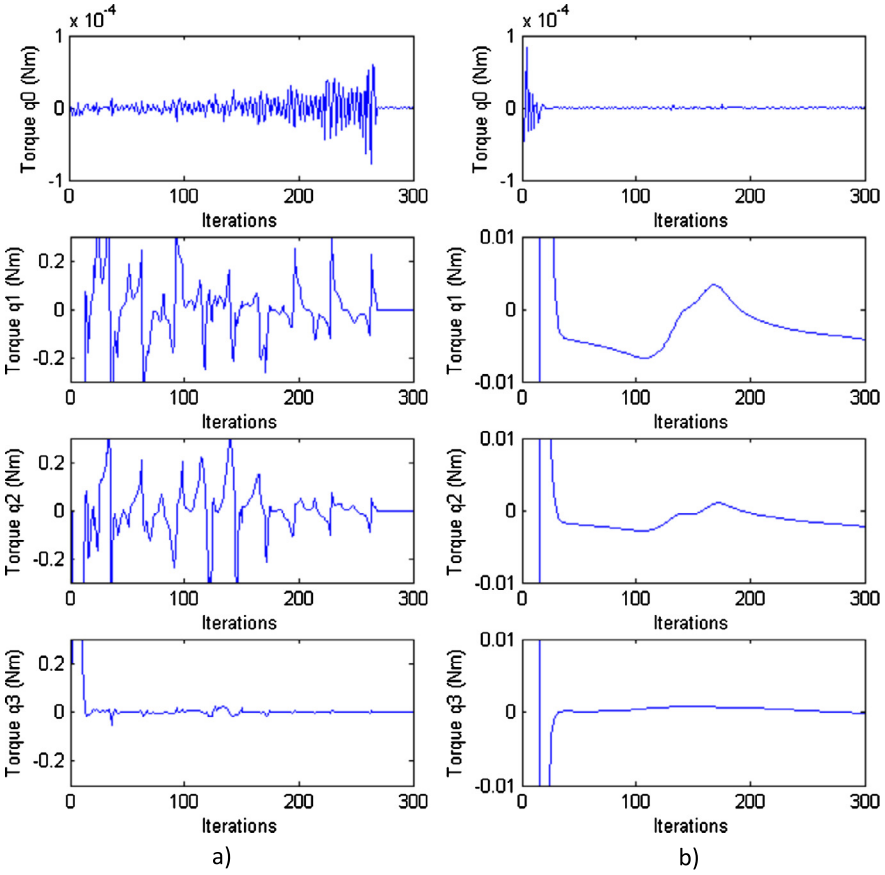

Fig. 6. Torque during the tracking. a) Without chaos control. b) With chaos control. Experiment 2.

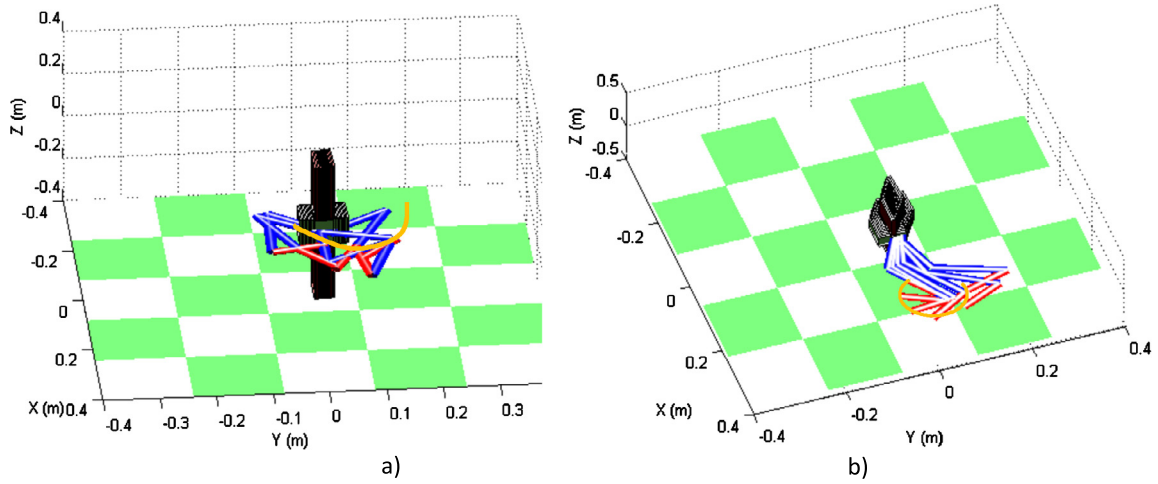

Fig. 7. 3D trajectory of the FFSMR. a) Without chaos control. b) With chaos control. Experiment 2.

Three different experiments with three different scenarios were developed, and the proposed controller worked properly for all of them. The first experiment illustrated the tracking of a non-repetitive image trajectory. The second one illustrated the tracking of a circular trajectory performed by the end-effector, where the chaotic movement of the joints was avoided by using the chaos compensator. Even though movements in 3D Cartesian space of the end-effector were very similar, when studying the torque applied to the joints, and thus, the evolution of the positions of the links, a great improvement was achieved, avoiding high fuel consumption due to sudden, fast, chaotic movements of the links. In the third experiment, the tracking of an abrupt trajectory was examined with the optimal control strategy with chaos compensation but with different values of the weight matrix.

Conflict of interest statement

There has been no conflict of interest in this work.

Acknowledgement

Research supported by the Spanish Ministry of Economy through the research project DPI2015-68087-R.

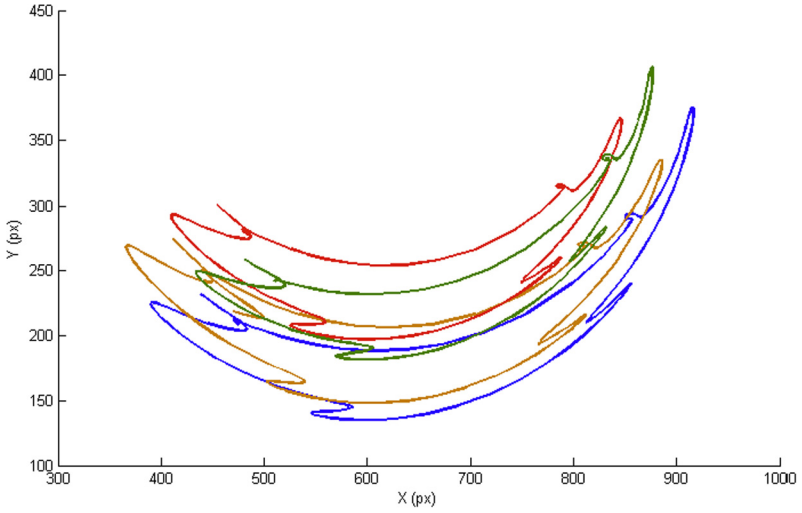

Fig. 8. Desired image trajectory. Experiment 3.

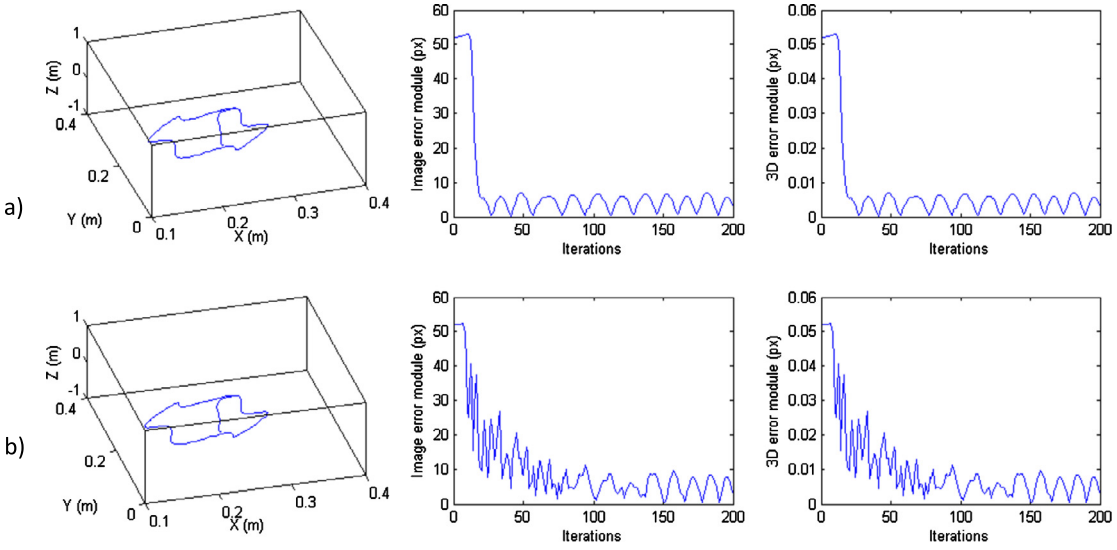

Fig. 9. 3D trajectory during the tracking of the desired image trajectory, image error module, and 3D error module. a) $W = (M^*_{mm})^{-1}$. b) $W = (M^*_{mm})^{-2}$. Experiment 3.

References

[1] A. Flores-Abad, O. Ma, K. Pham, S. Ulrich, A review of space robotics technologies for on-orbit servicing, Prog. Aerosp. Sci. 68 (2014) 1–26, http://dx.doi.org/10.1016/j.paerosci.2014.03.002.

[2] S. Dubowsky, E. Papadopoulos, The kinematics, dynamics, and control of free-flying and free-floating space robotic systems, IEEE Trans. Robot. Autom. 9 (1993) 531–543, http://dx.doi.org/10.1109/70.258046.

[3] F. Aghili, Pre- and post-grasping robot motion planning to capture and stabilize a tumbling/drifting free-floater with uncertain dynamics, in: 2013 IEEE Int. Conf. Robot. Autom., IEEE, 2013, pp. 5461–5468.

[4] F. Chaumette, S. Hutchinson, Visual servo control. I. Basic approaches, IEEE Robot. Autom. Mag. 13 (2006) 82–90, http://dx.doi.org/10.1109/MRA.2006.250573.

[5] A. Petit, E. Marchand, K. Kanani, Vision-based space autonomous rendezvous: a case study, in: 2011 IEEE/RSJ Int. Conf. Intell. Robot. Syst., IEEE, 2011, pp. 619–624.

[6] F. Chaumette, S. Hutchinson, Visual servo control. II. Advanced approaches [Tutorial], IEEE Robot. Autom. Mag. 14 (2007) 109–118, http://dx.doi.org/10.1109/MRA.2007.339609.

[7] A. Petit, E. Marchand, K. Kanani, Tracking complex targets for space rendezvous and debris removal applications, in: 2012 IEEE/RSJ Int. Conf. Intell. Robot. Syst., IEEE, 2012, pp. 4483–4488.

[8] F. Yu, Z. He, B. Qiao, X. Yu, Stereo-vision-based relative pose estimation for the rendezvous and docking of noncooperative satellites, Math. Probl. Eng. 2014 (2014) 1–12, http://dx.doi.org/10.1155/2014/461283.

[9] L. Song, Z. Li, X. Ma, Autonomous rendezvous and docking of an unknown tumbling space target with a monocular camera, in: Proc. 2014 IEEE Chinese Guid. Navig. Control Conf., IEEE, 2014, pp. 1008–1013.

[10] F. Aghili, A prediction and motion-planning scheme for visually guided robotic capturing of free-floating tumbling objects with uncertain dynamics, IEEE Trans. Robot. 28 (2012) 634–649, http://dx.doi.org/10.1109/TRO.2011.2179581.

[11] N. Inaba, M. Oda, M. Hayashi, Visual servoing of space robot for autonomous satellite capture, Trans. Jpn. Soc. Aeronaut. Space Sci. 46 (153) (2003) 173–179, http://dx.doi.org/10.2322/tjsass.46.173.

[12] N.R. Gans, G. Hu, W.E. Dixon, Keeping objects in the field of view: an underdetermined task function approach to visual servoing, in: 2008 IEEE Int. Symp. Intell. Control, IEEE, 2008, pp. 432–437.

[13] A.H.A. Hafez, V.V. Anurag, S.V. Shah, K.M. Krishna, C.V. Jawahar, Reactionless visual servoing of a dual-arm space robot, in: 2014 IEEE Int. Conf. Robot. Autom., IEEE, 2014, pp. 4475–4480.

[14] M. Sabatini, R. Monti, P. Gasbarri, G. Palmerini, Deployable space manipulator commanded by means of visual-based guidance and navigation, Acta Astronaut. 83 (2013) 27–43, http://dx.doi.org/10.1016/j.actaastro.2012.10.015.

[15] M. Jin, H. Yang, Z. Xie, K. Sun, H. Liu, The ground-based verification system of visual servoing control for a space robot, in: 2013 IEEE Int. Conf. Mechatronics Autom., IEEE, 2013, pp. 1566–1570.

[16] Y. Shi, B. Liang, X. Wang, W. Xu, H. Liu, Modeling and simulation of space robot visual servoing for autonomous target capturing, in: 2012 IEEE Int. Conf. Mechatronics Autom., IEEE, 2012, pp. 2275–2280.

[17] H. Yang, M. Jin, Z. Xie, K. Sun, H. Liu, Ground verification of space robot capturing the free-floating target based on visual servoing control with time delay, Ind. Robot 41 (2014) 543–556, http://dx.doi.org/10.1108/IR-05-2014-0339.

[18] G. Ma, Z. Jiang, H. Li, J. Gao, Z. Yu, X. Chen, et al., Hand-eye servo and impedance control for manipulator arm to capture target satellite safely, Robotica 33 (2015) 848–864, http://dx.doi.org/10.1017/S0263574714000587.

[19] M.D. Lichter, S. Dubowsky, State, shape and parameter estimation of space objects from range images, in: 2014 IEEE Int. Conf. on Robotics and Automation, vol. 3, 2014, pp. 2974–2979.

[20] U. Hillenbrand, R. Lampariello, Motion and parameter estimation of a free-floating space object from range data for motion prediction, in: 2015 Int. Symposium on Artificial Intelligence and Robotics & Automation in Space, i-SAIRAS, 2005.

[21] K. Yoshida, Engineering test satellite VII flight experiments for space robot dynamics and control: theories on laboratory test beds ten years ago, now in orbit, Int. J. Robot. Res. 22 (2003) 321–335, http://dx.doi.org/10.1177/0278364903022005003.

[22] J. Pomares, I. Perea, F. Torres, Dynamic visual servoing with chaos control for redundant robots, IEEE/ASME Trans. Mechatron. 19 (2014) 423–431, http://dx.doi.org/10.1109/TMECH.2013.2243160.

[23] K. Pyragas, Delayed feedback control of chaos, Philos. Trans. R. Soc. 364 (1846) (2006) 2309–2334, http://dx.doi.org/10.1098/rsta.2006.1827.

[24] J. Pomares, I. Perea, C.A. Jara, G.J. García, F. Torres, Dynamic visual servo control of a 4-axis joint tool to track image trajectories during machining complex shapes, Robot. Comput.-Integr. Manuf. 29 (2013) 261–270, http://dx.doi.org/10.1016/j.rcim.2013.01.008.

[25] Y. Mezouar, F. Chaumette, Design and tracking of desirable trajectories in the image space by integrating mechanical and visibility constraints, in: 2001 IEEE Int. Conf. on Robotics and Automation, vol. 1, ICRA'01, 2001, pp. 731–736.